Atmos. Chem. Phys., 10, 4741–4756, 2010
www.atmos-chem-phys.net/10/4741/2010/
doi:10.5194/acp-10-4741-2010

Atmospheric Chemistry and Physics

Improvements in the profiles and distributions of nitric acid and nitrogen dioxide with the LIMS version 6 dataset

E. Remsberg[1], **M. Natarajan**[1], **B. T. Marshall**[2], **L. L. Gordley**[2], **R. E. Thompson**[2], **and G. Lingenfelser**[3]

[1]NASA Langley Research Center, 21 Langley Blvd., Mail Stop 401B, Hampton, VA 23681 USA
[2]GATS Incorporated, 11864 Canon Blvd., Suite 101, Newport News, VA 23606 USA
[3]SSAI, 1 Enterprise Parkway, Hampton, VA 23661 USA

Received: 14 December 2009 – Published in Atmos. Chem. Phys. Discuss.: 3 February 2010
Revised: 11 May 2010 – Accepted: 13 May 2010 – Published: 26 May 2010

Abstract. The quality of the Nimbus 7 Limb Infrared Monitor of the Stratosphere (LIMS) nitric acid (HNO_3) and nitrogen dioxide (NO_2) profiles and distributions of 1978/1979 are described after their processing with an updated, Version 6 (V6) algorithm and subsequent archival in 2002. Estimates of the precision and accuracy of both of those species are developed and provided herein. The character of the V6 HNO_3 profiles is relatively unchanged from that of the earlier LIMS Version 5 (V5) profiles, except in the upper stratosphere where the interfering effects of CO_2 are accounted for better with V6. The accuracy of the retrieved V6 NO_2 is also significantly better in the middle and upper stratosphere, due to improvements in its spectral line parameters and in the reduced biases for the accompanying V6 temperature and water vapor profiles. As a result of these important updates, there is better agreement with theoretical calculations for profiles of the HNO_3/NO_2 ratio, day-to-night NO_2 ratio, and with estimates of the production of NO_2 in the mesosphere and its descent to the upper stratosphere during polar night. In particular, the findings for middle and upper stratospheric NO_2 should also be more compatible with those obtained from more recent satellite sensors because the effects of the spin-splitting of the NO_2 lines are accounted for now with the LIMS V6 algorithm. The improved precisions and more frequent retrievals of the LIMS profiles along their orbit tracks provide for better continuity and detail in map analyses of these two species on pressure surfaces. It is judged that the chemical effects of the oxides of nitrogen on ozone can be studied quantitatively throughout the stratosphere with the LIMS V6 data.

Correspondence to: E. Remsberg
(ellis.e.remsberg@nasa.gov)

1 Background

The Limb Infrared Monitor of the Stratosphere (LIMS) experiment was launched on 24 October 1978 on the near polar-orbiting Nimbus 7 satellite. LIMS operated from 25 October until 28 May 1979, measuring vertical radiance profiles across the atmospheric limb of the Earth (Gille and Russell, 1984). Single limb radiance profiles were measured about every 12 seconds along an orbital track of the LIMS tangent point locations. Its daily orbital data extend from 64° S to 84° N and are available at two local times per latitude (at about 1300 h and 2300 h at the Equator). The radiances were processed to infer middle atmospheric temperature profiles and the concentrations of several chemical compounds important for the chemistry of stratospheric ozone. LIMS provided profiles of ozone (O_3), water vapor (H_2O), nitric acid (HNO_3), and nitrogen dioxide (NO_2). Thus, LIMS was the first satellite experiment to provide a simultaneous, near-global view of the key chemical compounds in the ozone/nitrogen oxide photochemical chain. The temperature, geopotential height, and constituent profiles have been used for many scientific investigations, including effects of radiation on the net transport (Mlynczak et al., 1999), responses of the middle atmosphere to perturbations (Leovy et al., 1985), and correlations between the temperature and species data (Froidevaux et al., 1989).

The LIMS Version 5 (or V5) profile dataset was archived in 1982; its measurements, algorithms, and data products are described in Gille and Russell (1984) and references therein. Since that time, significant improvements have been realized in the original spectroscopic parameters (Drayson et al., 1984) that were used for the V5 retrieval of temperature/pressure or T(p) and for the gaseous constituent profiles

Published by Copernicus Publications on behalf of the European Geosciences Union.

Table 1. Calculations of precision and accuracy (%) for LIMS V6 HNO_3.

Pressure (hPa)	80	50	30	10	3
Random (PRECISION)	21	4	3	3	10
Calibration	1	1	2	1	7
Temperature Bias	5	1	3	1	6
Spectral Band Model Error	5	5	5	5	5
CFC & Aerosol Corrections	5	5	2	1	1
Registration & Forward Model Errors	13	6	5	5	5
Root-Sum-Squares (RSS) of bias errors (ACCURACY)	16	9	8	7	12
Unverified Sources of Error					
FOV Side Lobes	27	28	25	27	45
Out-of-band Spectral Signal	29	29	20	7	45

that contribute to the radiances measured within the six channels of LIMS. For this reason a reprocessing of the LIMS Level 2 (or profile) data to Version 6 (V6) was considered for several of its primary and interfering gases using the line parameters of HITRAN 92 (Rothman et al., 1992a). As a result, these V6 data are considered more appropriate for comparisons with the temperature and species distributions obtained from the several middle atmosphere instruments onboard the NASA Upper Atmosphere Research Satellite (UARS), the Earth Observing System (EOS) Aura satellite and on the Canadian, European, and/or Japanese satellites SCISAT, ODIN, ENVISAT, and ADEOS.

The V6 dataset contains improvements due to a better knowledge of the orbital attitude for the LIMS measurements, from the application of a multiple interleave retrieval process, and from using all the radiance profile samples, spaced 0.375 km in altitude. Descriptions of the V6 algorithms for the conditioned radiances of all the channels and for the retrieval of the temperature and geopotential height profiles are in Remsberg et al. (2004). Characterizations of the improvements for V6 ozone and water vapor are provided in Remsberg et al. (2007, 2009). This paper is focused on the improvements and scientific implications for the V6 HNO_3 and NO_2 profiles and distributions.

The LIMS instrument is essentially a limb-viewing radiometer, and the optical characteristics of all the channels are given in Russell and Gille (1978, their Table 1). A single LIMS scan profile begins with the center of its field-of-view (FOV) array viewing the horizon at 153 km altitude, moving steadily downward to a point 38 km below the solid Earth limb and then returning upward in the same manner. The angular resolutions (in milliradians or mrad) for the detectors of the FOV array are 1 mrad for the NO_2 and H_2O channels and 0.5 mrad for the other four LIMS channels, including HNO_3. Their instantaneous FOV at the horizon is 3.6 km for NO_2 and H_2O and 1.8 km for HNO_3, O_3, and for temperature from its two CO_2 channels. Radiance samples are obtained every 0.375 km in altitude for HNO_3 and 0.75 km for NO_2. The filter for the LIMS HNO_3 channel extends from 842 to 915 cm^{-1}, its 5% transmission points. That channel measured the radiance emitted by the ν_5 and $2\nu_9$ bands or in the region of 11.3 µm. The V6 HNO_3 retrievals were obtained using the same laboratory-measured, band parameters used to process the LIMS V5 profiles (Drayson et al., 1984; Goldman et al., 1981). Thus, the primary improvements for V6 HNO_3 occur in the upper stratosphere due to accounting for the CO_2 laser band emission centered near 10.4 µm and in the lower stratosphere from the underlying emissions of the CFCs and aerosols. The filter for the LIMS NO_2 channel has its 5% transmission points at 1561 and 1631 cm^{-1}. The effects of the spin splitting for its lines are included in the line parameters of HITRAN 92 that we used (Rothman et al., 1992a). The band intensity for the primary $NO_2\,\nu_3$ cold band of HITRAN 92 was also unchanged for HITRAN 96 (Rothman et al., 1998), although the strengths of its assigned lines are altered somewhat in HITRAN 96 based on the analyses of Toth (1992).

The LIMS retrievals make use of an onion-peeling approach along with the emissivity growth approximation (EGA) of Gordley and Russell (1981). The V6 Level 2 data files contain both the de-convolved radiances and the retrieved parameters, and they are tabulated at 18 levels per decade of pressure or at a spacing of about 0.88 km. Note that the UARS Level 3A profiles have 6 levels of data per decade of pressure and represent a matching subset to the LIMS V6 data for easy comparison. In addition, the time, location, and solar zenith angle for the tangent point of a LIMS measurement are included in the header lines of each profile. This information makes it easier to relate the LIMS profiles of O_3, HNO_3, and NO_2 to photochemical model output. The effective vertical resolution for both V6 HNO_3 and NO_2 is of order 3.7 km, and retrievals were performed for each of the down/up scan pairs spaced about 1.6 degrees of latitude along the LIMS orbital tangent tracks. Distributions of HNO_3 extend from near the tropopause to just above the 2-hPa level. The nighttime distributions of NO_2 extend from

about 50 hPa to the lower mesosphere, especially for the polar night. Results for daytime NO_2 are useful from about 50 hPa to 1 hPa.

Section 2 shows several daily, zonally-averaged distributions of the V6 HNO_3 and NO_2 for comparisons with model output and with distributions from more recent satellite experiments that also were observing during periods when the stratospheric aerosol loading was near background levels. An extensive validation of the V6 products was not conducted, although their daily zonal mean cross sections have been assessed against those of the V5 data that had been compared with the few correlative measurements available during the LIMS timeframe (e.g., Gille et al., 1984; Gille, 1987; Russell et al., 1984a; Remsberg and Russell, 1987). Qualitative improvements have been found for all the V6 data products.

Section 3 describes the significant changes in the V6 algorithm that affect the V6 HNO_3 and NO_2 profiles. Precision and accuracy for those V6 data are included, based on calculations of the effects of their known error sources. These calculated precisions are shown to compare well with the variations in the retrieved HNO_3 and NO_2 from among adjacent scans along an orbit, specifically for latitudes and times when zonal variations due to wave activity were minimal. Section 4 presents some scientific findings demonstrating the improved quality of the V6 HNO_3 and NO_2. Section 5 is a summary of findings about the changes with V6.

2 Zonally-averaged distributions of HNO_3 and NO_2

There were 13 to 14 orbits of data per day from LIMS, following the Sun-synchronous geometry for the Nimbus 7 satellite (Gille and Russell, 1984). Retrievals were performed on the radiance profiles, located along the ascending (south-to-north) and the descending (north-to-south) node, tangent tracks of each orbit. The local time of a measurement at the low and middle latitudes is near 1 p.m. for the ascending node and 11 p.m. for the descending node data. As an introduction, we show several V6 HNO_3 and NO_2 distributions obtained from the LIMS Level 2 profiles.

Figure 1 provides the daily, zonally-averaged distributions of V6 HNO_3 from the combination of its species profiles from the descending and ascending orbital segments for 15 November 1978, (top panel) and 16 May 1979 (bottom panel). Maximum mixing ratio values occur at the high latitudes near 30 hPa, and the variation of HNO_3 with latitude is similar to that from the earlier V5 dataset at that pressure level (Gille et al., 1984, 1993). However, the V6 HNO_3 profiles no longer show nearly constant values in the upper stratosphere, as was the case for V5 in Jackman et al. (1985). This improvement is due primarily to a better accounting for the effects of the interfering radiance from the laser band of carbon dioxide (CO_2) at 10.4 µm. The V6 HNO_3 agrees reasonably well with the photochemical model estimates of Jackman et al. (1985). The LIMS V6 daytime values are

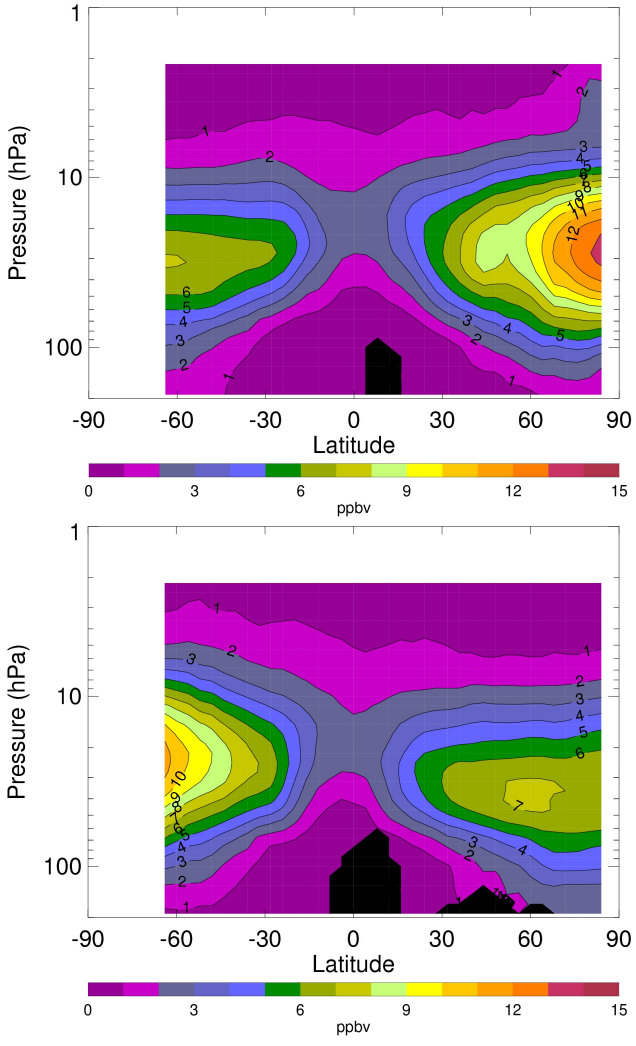

Fig. 1. V6 HNO_3 distributions in ppbv for (top) 15 November 1978 and (bottom) 16 May 1979, based on a combination of the profile data from their ascending and descending orbital segments. Orange-to-red colors represent high values and magenta colors are low values; blackened regions indicate where there are no data.

slightly less than its nighttime values near the 4-hPa level (not shown), possibly due to not having accounted accurately for the effects of the temperature tides on the LIMS HNO_3 radiances. V6 HNO_3 values are somewhat smaller than those of V5 in the tropical lower stratosphere, due to first-order corrections in the V6 algorithm for the effects of interfering emissions from aerosols and from the chlorofluorocarbon (CFC) molecules $CFCl_3$ and CF_2Cl_2. The 1 ppbv contour extends to just above the 50-hPa level at equatorial latitudes; that value is at the upper limit of reactive nitrogen (NO_y) minus odd nitrogen (NO_x) from in situ measurements (e.g., Jensen and Drdla, 2002, and references therein).

One can see from Fig. 1 that there is very good seasonal symmetry between the HNO_3 distributions of the middle and

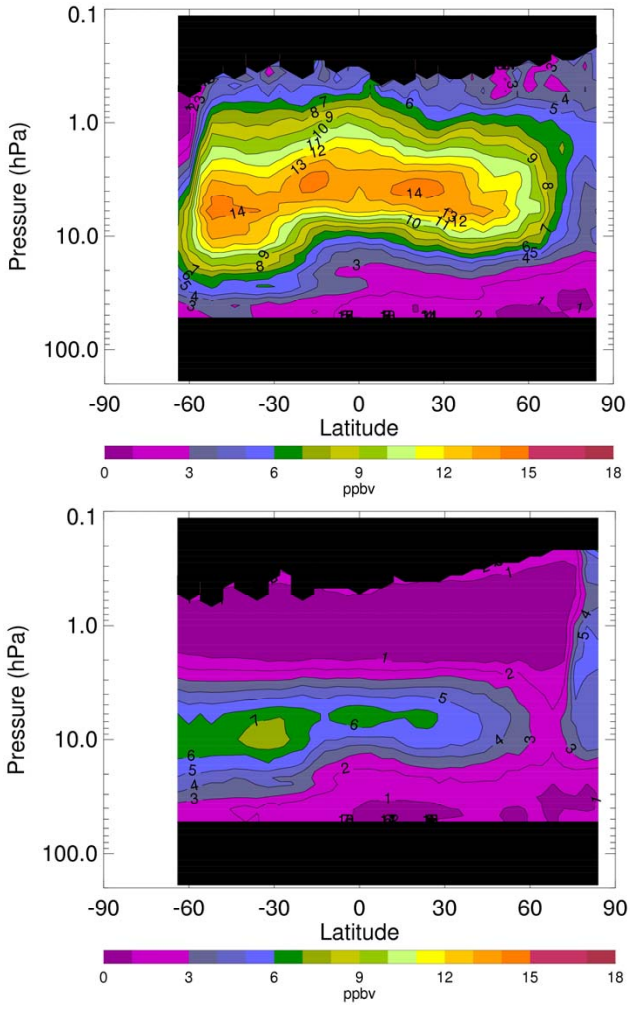

Fig. 2. LIMS V6 distributions for 15 November 1978 of (top) descending (or nighttime) NO_2 and of (bottom) ascending (or daytime) NO_2 both in ppbv. Orange colors are high values, while magenta-to-purple colors are low values; blackened regions indicate where there are no data. There is a crossover to polar night conditions at about 75° N for the ascending NO_2.

lower stratosphere for November versus May of the northern and southern hemispheres. Austin et al. (1986) explained that the increases in fall and winter were likely a result of heterogeneous, chemical production mechanisms. Note that the values of HNO_3 are also larger in November at high northern latitudes of the upper stratosphere (top panel of Fig. 1). This feature becomes even more prominent in midwinter due to an accumulation of HNO_3 from a chemical conversion of NO_2 and di-nitrogen pentoxide (N_2O_5) under polar night conditions (e.g., Kawa et al., 1995; Bekki et al., 1997; Stiller et al., 2005). The distribution of 16 May (bottom panel of Fig. 1) also indicates that there was an accumulation of HNO_3 in the lower part of the northern, polar stratosphere from the winter and early spring.

Because NO_2 undergoes large diurnal variations in the upper stratosphere, Fig. 2 shows its zonal-averages from the descending (or local nighttime at low and middle latitudes – top panel) and from the ascending (or local daytime at low and middle latitudes – bottom panel) orbital segments for 15 November 1978. Maximum mixing ratio values for the nighttime LIMS NO_2 of Fig. 2 (top panel) are of the order of 14 ppbv centered at about the 4-hPa level. The retrieved nighttime NO_2 profiles extend into the lower mesosphere, where they encounter their signal-to-noise (S/N) limit and are less accurate. The repartitioning of the NO_x (nitric oxide (NO)+NO_2) at twilight occurs at about 55 to 60° S latitude. Those terminator NO_2 profiles are also less accurate because their rapidly changing NO_2 values along the tangent path were not accounted for in the same manner as in Solomon et al. (1986).

Maximum mixing ratios for the ascending NO_2 (daytime at most latitudes) of Fig. 2 (bottom panel) are of the order of 6 to 7 ppbv and occur between 8 and 10 hPa. Note that there is a crossover to polar night conditions at about 75° N. The daytime NO_2 at the lower latitudes is small in the upper stratosphere because most of the NO_x is in the form of NO. H_2O emission becomes a significant part of the NO_2 channel radiance in the upper stratosphere, especially during daytime. The forward radiance model for the V6 NO_2 channel assumes that H_2O has a constant value of 6.5 ppmv above the upper limit of 1.3 hPa for its V6 profile. Furthermore, there is a significant amount of extra emission in the mesosphere during daylight from excited states of the H_2O molecule that are difficult to characterize for LIMS, primarily because its ground-state H_2O populations are not known exactly for those altitudes (Lopez-Puertas and Taylor, 2001; Kerridge and Remsberg, 1989). For this reason no corrections for non-LTE effects from H_2O were developed for the retrieval of the V6 NO_2. That source of positive radiance bias is the most likely reason for the spurious, upward extension of the daytime NO_2 distributions above the 1-hPa level from 64° S to ∼70° N (see also Sects. 3 and 4).

Figure 3 is the distribution of NO_2 from the descending (nighttime) orbital segments of 15 January 1979, and it is similar to that of Fig. 2 (top panel) in most respects. One exception is the occurrence of larger values of NO_2 in the upper stratosphere near 50° S in Fig. 3 than in Fig. 2. This difference is partly a diurnal effect. The LIMS NO_2 measurements for the descending orbital segments were obtained at about 2130 h (local time) at 50° S versus 2300 h at the equator, and there is a steady conversion of NO_2 to N_2O_5 from just after sunset and until sunrise. Furthermore, sunset occurs later in the day during summer at the high southern latitudes.

The elevated values of NO_2 in the mesosphere at the high latitudes of the northern hemisphere are another feature of Fig. 3. Such enhanced values of NO_2 were first reported by Russell et al. (1984b) based on a special, radiance-averaged version of the LIMS data, and they were attributed to the formation of NO_x in the mesosphere followed by a gradual

descent of the air to the uppermost stratosphere during polar night. Findings from more recent satellite sensors support that interpretation (e.g., Randall et al., 2009). A time series of the V6 polar night NO_2 will be shown in Sect. 4, indicating the improved estimates for its values and a better continuity for its descent during the winter months of 1978/1979.

3 LIMS V6 retrieval algorithms and error estimates

3.1 The V6 algorithms for HNO_3 and NO_2

Emissivity data tables for the forward limb-radiance algorithms were developed as a function of temperature and pressure for each of the gases that make contributions in the HNO_3 and NO_2 channels. The V6 forward model for HNO_3 makes use of the cross section parameters of Goldman et al. (1981), based on the laboratory measurements of Giver et al. (1984). That parameterization is appropriate for the broadband HNO_3 channel of LIMS, and it is essentially unchanged from that used for V5. Although there were uncertainties associated with the line parameters on the HITRAN HNO_3 databases during the 1990s, it is noted that the HNO_3 line intensities in the 11-μm region for HITRAN 96 also include normalizations to the band intensities of Giver et al. (1984).

The HNO_3 channel contains secondary radiance contributions from the laser band of CO_2 at 10.4 micrometers and from the primary CFCs ($CFCl_3$ and CF_2Cl_2). The line parameters for CO_2 were taken from HITRAN 92 (Rothman et al., 1992a and b; Dana et al., 1992), which are improved over the parameters used with the original LIMS V5 algorithm. To achieve better accuracy for the emissivity of CO_2 along a tangent ray path, its emissivity table values were generated at 55 pressure levels and 33 temperature levels encompassing their expected atmospheric ranges. In addition, polynomial fits were not used to account for the temperature dependence within the emissivity tables; linear interpolation was employed instead. These upgrades have led to a more accurate representation of the effects of the laser band of CO_2. To summarize, the V6 emissivity tables for CO_2 account for much of the excess of retrieved HNO_3 that characterized the V5 HNO_3 profiles from about 5 to 2 hPa, as originally reported in Gille et al. (1984), Jackman et al. (1985), and Gille et al. (1993) (see also Sect. 4).

Line parameters for the original V5 retrievals of NO_2 were obtained from the AFGL trace gas compilation (Rothman et al., 1981). Later, the spin-rotation effects of NO_2 were identified, and the fine structure of the lines for the primary ν_3 cold band was included in the HITRAN 92 compilation via a perturbation calculation (Perrin et al., 1992). This update accounts for most of the improvements in the V6 NO_2 profiles (Remsberg et al., 1994). Only minor changes in the retrieved NO_2 are expected from the more explicit calculations of the strengths of those resolved lines reported by Toth (1992)

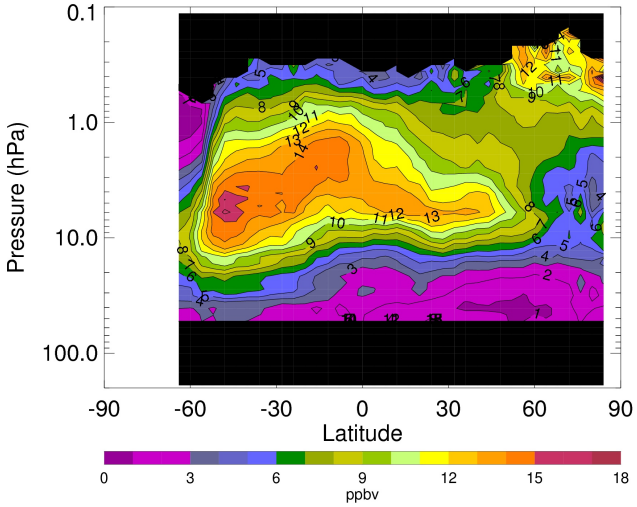

Fig. 3. As in the top panel of Fig. 2, but for descending (or nighttime) NO_2 in ppbv for 15 January 1979. Orange-to-red colors are high values and magenta-to-purple colors are low values; blackened regions are where there are no data.

and available later in HITRAN 96. The LIMS NO_2 channel also contains contributions from H_2O, CH_4, and the oxygen (O_2) continuum, and tables were developed for each of them. Since the LIMS NO_2 radiances are interfered with substantially by H_2O in the stratosphere, an additional emissivity table was employed to account for the effects of their overlapping lines (Remsberg et al., 2004). Spectral parameters for the underlying O_2 were not available, so the empirical model of Thibault et al. (1997) was used for consistent calculations of the effects of the continuum-induced O_2 absorption in both the LIMS H_2O and NO_2 channels.

The LIMS V6 profiles were used to correct for the forward radiance contributions of H_2O in the NO_2 channel up to about the 1.5-hPa level, and then they were extended upward using a constant value of 6.5 ppmv. In addition, the entire H_2O profile for the forward model was smoothed by a Gaussian function having a half-width of 1.5 km at half maximum. As indicated earlier, no corrections were developed to account for non-LTE radiances from mesospheric H_2O during daytime. Even so, there is no indication of a bias in the retrieved NO_2 due to that neglect, except at and above about 48 km (near 1 hPa). Emissions from excited states of daytime NO_2 were postulated for the upper stratosphere by Kerridge and Remsberg (1989), but no corrections for those effects were developed for V6 because the populations of those states were not known well. More importantly, Funke et al. (2005a) reported finding no evidence for such non-LTE effects in upper stratospheric NO_2 from the higher spectral-resolution data of MIPAS on the ENVISAT satellite. The effects of horizontal mixing ratio gradients in the tangent layer were shown to be important for the retrieval of LIMS NO_2 in the region of the day/night terminator (Solomon et al., 1986).

However, because such a gradient correction is needed only for solar zenith angles near 90 degrees, a second-pass processing was not applied to the V6 NO_2 profiles prior to their archival in 2002.

Estimated concentrations of the interfering gases were obtained as follows. Updated, seasonal zonal-mean distributions of CH_4 were generated from the UARS HALOE dataset for use with the V6 retrievals of NO_2 but with an extrapolation of their magnitudes back to 1979, based on the approximate, linear emission rate for CH_4 at the ground. A similar extrapolation was performed for $CFCl_3$ and CF_2Cl_2 for the HNO_3 channel, based on their measured distributions from the UARS CLAES Version 8 dataset plus knowledge of the growth rates for their emissions since 1975. Interfering emission due to aerosols has its largest effect on the LIMS-retrieved HNO_3 at low latitudes of the lower stratosphere. Zonal mean distributions of the background aerosol extinction were not available for the seven months of LIMS, and its V5 dataset had no correction for it. A first-order aerosol extinction cross section was generated for the V6 algorithm, based on estimates for the background stratospheric aerosol layer of 1978/1979. Specifically, a single zonal-mean distribution of aerosol extinction was adopted, based on March/May 1996 results for the HALOE 5.26 µm (nitric oxide or NO) channel (Hervig et al., 1995). The magnitude of that distribution was then scaled back to 1978/1979 using a factor obtained by comparing the SAGE II 1-µm channel aerosol extinction values of 1996 versus the SAGE I aerosol extinction for the same months of 1979. That single modified, zonal mean aerosol distribution was used for each of the seven months of the LIMS dataset and must be considered as somewhat qualitative with latitude and not truly representative of its seasonal cycle variations. Since tropical aerosol extinctions vary most noticeably according to the phase of the QBO cycle (Hitchman et al., 1994), a scaling of their values between the 1996 and the 1979 March/May periods was used because they occurred at nearly the same QBO phase. Finally, aerosol extinctions at the wavelengths of the LIMS channels versus that at 5.26 µm of HALOE were obtained by employing the sulfuric acid/H_2O composition and the wavelength-dependent, refractive index model for its aerosol absorption in the manner of Hervig et al. (1995).

The original V5 profiles of NO_2 and HNO_3 were used as a priori estimates for the V6 forward models, although there is no dependence upon them for the onion-peeling retrievals of LIMS once a reasonable S/N level for the radiances was met. The archived V6 profiles were screened for anomalies using several criteria. First, the retrieval process for a tangent layer value was iterative. The variances between successive iterations were calculated, and they were checked for convergence to near the measurement noise. Those variances are defined in terms of $(NEN/K)^2$, where NEN is the noise equivalent radiance for each channel in watts/m^2-sr (Gille and Russell, 1984) and K is the derivative of the measured signal profile as a function of the given species mixing ratio. Variances were set to the negative of their actual values whenever convergence was not achieved or the retrieval needed to be restarted (at tops of profiles). Valid profile segments have positive variances, and only the retrieved values from those segments were retained in the final Level 2 output file. Variance limits effectively set the extreme upper altitude of the good data for each of the parameters. Negative variances often indicate the low altitude extent of good data, too. Variance checking occurred primarily outside of the pressure ranges of 1.9 hPa to 46 hPa for HNO_3 and of 0.88 hPa to 46 hPa for NO_2. Independent estimates of the random error indicate that there is adequate tangent layer signal within those ranges. An additional algorithm was applied to identify and screen for contaminating radiances from cloud tops. The profiles of HNO_3, H_2O, and NO_2 were also screened for polar stratospheric cloud features prior to their archival, based on the occurrence of those features in the retrieved ozone profiles (Remsberg et al., 2007).

Species profile segments were also screened within given pressure ranges, when their retrieved mixing ratios exceeded certain threshold values. The pressure range for HNO_3 was 2.2 to 46 hPa and its threshold was 30 ppbv; only a very few points met that criterion, and they were judged to be spurious. H_2O is a major interference for the retrieval of NO_2, particularly in the polar lower stratosphere during winter; its screening threshold was set at 12 ppmv over the pressure range of 1.47 to 46 hPa. Unrealistically, large values of H_2O can occur due to not resolving the temperature structure properly. NO_2 thresholds were set for two separate pressure regions. Those thresholds were 25 ppbv within 1 to 31.6 hPa or 10 ppbv within 36 to 68 hPa, neither of which would be explained by an excess in the retrieved H_2O. Almost all the profiles where NO_2 exceeded 25 ppbv in the upper stratosphere occurred in early December 1978 or in January 1979, when their temperature structures were associated with stratospheric warming events. The retrieved LIMS H_2O and NO_2 values are not very accurate in that case. Quantitative studies of the descent of NO_2 from the mesosphere to the stratosphere can be affected somewhat by this 25 ppbv limit, although time series of the retrieved NO_2 for the upper stratosphere do not indicate any bias (see also Sect. 4.4). Further, it is noted that no screening threshold was applied to the retrieved NO_2 of the polar mesosphere. Information about specific profile segments that were screened can be found on the LIMS Website (http://lims.gats-inc.com) for each day of the LIMS V6 dataset.

3.2 Single profile error estimates

The V6 HNO_3 profile values are not much different from those of V5, except in the upper stratosphere where the interference from CO_2 has been accounted for better in the V6 algorithm. In the tropical lower stratosphere there are important differences due to the corrections for emissions from the CFCs and due to the first-order correction for the aerosol

emission. Random radiometric errors for V6 HNO_3 are reduced from those of V5 by a factor of 2.2 because of the larger number of samples used with the interleave procedure for the retrieval of a V6 profile (Remsberg et al., 2004). Offset errors due to pointing jitter are included in those random uncertainties. The calculated precisions vary from 0.15 ppbv at 80 hPa to 0.05 ppbv at 3 hPa, based on an average profile at 30° S. Those calculated values are provided in percent in the top row of Table 1, and they compare well with empirical estimates of the precision from the Level 2 data themselves (the standard deviation (SD) profile in Fig. 4). The SD values were obtained as the minimum of the variances for each pressure level from among the sets of scans along each of the orbits that crossed 25° S to 35° S latitude on 1 February 1979. Of course, a part of the empirical SD values in Fig. 4 may be a result of real variations in the atmospheric HNO_3.

Sources of systematic uncertainty were reported in Gille et al. (1984), based on simulations of their effects for V5 from a model HNO_3 profile for 32° N. Many of those error estimates are retained for V6, as shown in the middle rows of Table 1. However, the effects of temperature bias are based on the revised estimates of T(p) error in Remsberg et al. (2004). Uncertainty for the spectral band model is 5%, according to Goldman et al. (1981). Uncertainties in the aerosol and CFC corrections are greatest for the tropical lower stratosphere but do not dominate the total error during 1978/1979. Biases at the tops of the V6 HNO_3 profiles are small because its a priori mixing ratio values are small near the stratopause, and they are applied above the pressure level of the first retrieved point, too. Uncertainties for the effects of the horizontal temperature gradients are not included, since sensitivity to temperature biases are relatively small for an optically thin species like HNO_3.

The largest elements of potential bias error are the ±20% uncertainties in the integrated areas of the field-of-view (FOV) side lobes and from a possible 0.05% bias in the total measured signal due to regions of the channel filter that are outside the main spectral band, as discussed in Gille et al. (1984) and shown in the bottom rows of Table 1. The FOV side lobes from the HNO_3 channel are not all the same sign. To judge their effects, the measured HNO_3 radiance profiles were analyzed at the vertical distances of the side lobes from the main HNO_3 lobe or at effective separations of 17 and 34 km at the horizon. For instance, are there any positive or negative radiance correlations at those separations when the main lobe is viewing the low radiances of the mid to upper stratosphere and when the side lobes are viewing the much larger radiances at altitudes 17 or 34 km below? Our investigations indicated no significant correlations for HNO_3 below 40 km. Thus, it is concluded that the magnitude of that error in Table 1 must be an upper limit at all levels, except perhaps at 3 hPa. Uncertainties for the out-of-band spectral response can impart a positive bias in HNO_3 of order 20% at 30 hPa, as pointed out in Gille et al. (1984). Yet, qualitative comparisons with other HNO_3 datasets indicate agreement

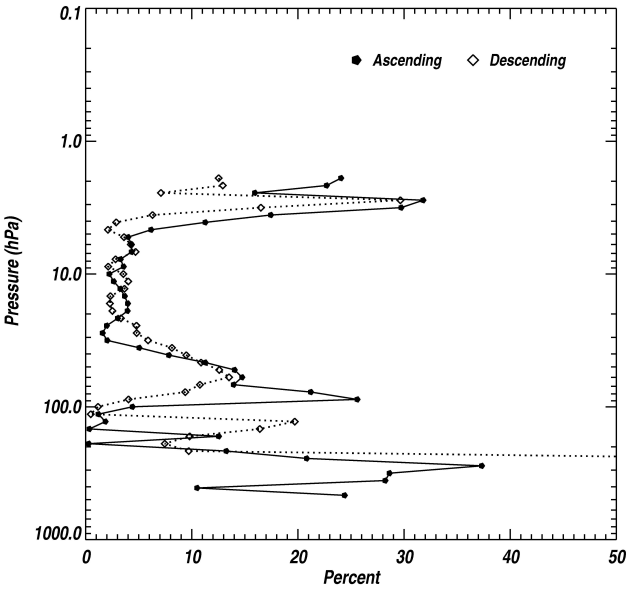

Fig. 4. Estimates of precision based on the minimum standard deviations (SD) of the retrieved LIMS V6 HNO_3 profiles from the sets of ascending (solid) or descending (dashed) orbital crossings of the latitude band of 25° S and 35° S on 1 February 1979.

that is better than 20%, at least for those datasets that were obtained at times of relatively low stratospheric aerosol loading. Therefore, neither of those sources of error is included in the combined root-sum-squares (RSS) calculations of accuracy in Table 1. In summary, the overall accuracy for V6 HNO_3 is believed to be very good from 30 hPa to 10 hPa or of order 10% at middle latitudes.

Table 2 contains the calculations of precision and accuracy for the profiles of NO_2. First, one is reminded that the nighttime values of V6 NO_2 have peak mixing ratios near 4 hPa that are about 15% to 20% lower than those of V5. Most of that change is due to the effects of the spectral spin splitting of the strong lines that were not considered for earlier versions of the AFGL or HITRAN line lists. On the other hand, the peak daytime V6 NO_2 values at 8 to 10 hPa are reduced from V5 by only about 5% because the effect of saturation for the strongest lines is not nearly so pronounced for the lower mixing ratios of daytime. In the upper stratosphere near 3 hPa, the daytime V6 NO_2 is larger than that of V5 due to the improved determinations of the interfering V6 H_2O. Below the 30-hPa level of the lower stratosphere both the day and night V6 NO_2 values are somewhat larger than V5. At this point it is noted that the V5 algorithm contained a merger of its retrieved NO_2 with a balloon-based, average NO_2 profile from 30° N, constraining its results below the 30-hPa level at least when the S/N for the tangent-layer radiance was low. The V6 NO_2algorithm is not constrained by any such climatological profile.

Table 2. Calculations of precision and accuracy (%) for LIMS V6 NO_2.

Pressure (hPa)	50	30	10	5	3	1
Noise and offset error	5	5	3	3	3	14
H_2O interference	3	3	3	3	5	–
Random (Root-Sum- Squares or RSS Value – PRECISION)	6	6	4	4	6	14
Radiometric Bias Errors	6	6	6	6	6	6
Temperature Bias	22	13	8	8	6	10
H_2O Mixing Ratio	30	13	6	6	8	28
O_2Cross Section (10%)	34	18	3	1	0	0
NO_2 Line Parameters (10%)	10	10	10	10	10	10
Algorithm/Registration	13	6	5	5	5	5
Main FOV Lobe	5	5	5	5	5	5
RSS of Bias Errors (ACCURACY)	53	29	18	18	17	33
Unverified Source of Error (FOV Side Lobe Area)	1	2	4	1	2	1

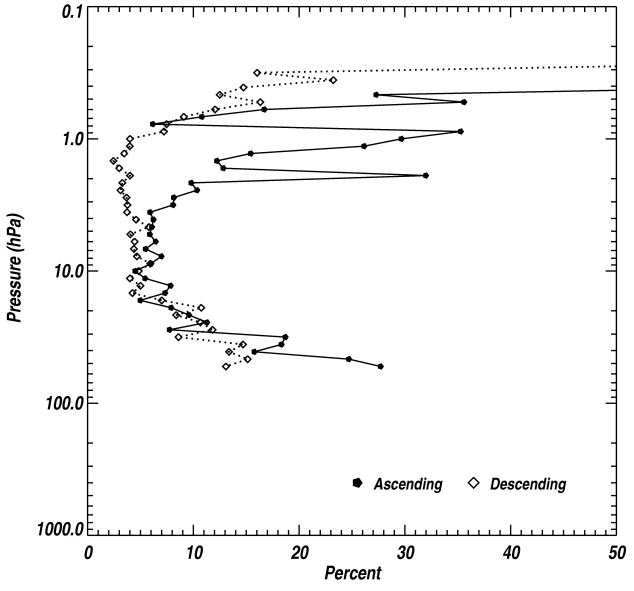

Fig. 5. As in Fig. 4, but for estimates of precision (SD) for LIMS V6 NO_2 profiles.

The calculated precision values for the V6 NO_2 in Table 2 were adopted from those of V5 in Russell et al. (1984a), after accounting for the improvements due to the use of all the samples within the measured radiance profiles. Random uncertainties from single profiles of the retrieved H_2O were adopted from Remsberg et al. (2009) and are included because H_2O is a major source of interfering emission, especially for daytime NO_2 in the upper and the lowermost stratosphere. The effects of those random H_2O errors are scaled further, according to the fraction of the signal in the NO_2 channel that is due to H_2O. Estimates of percentage NO_2 precision profiles from the data are shown in Fig. 5 and are based on average daytime and average nighttime SD profiles at 30° S for 1 February 1979. Those values range from about 5% in the middle stratosphere, to 8% for nighttime or 30% for daytime at 1 hPa, and then to 15–20% at 40 hPa. The estimated SD values in Fig. 5 agree with the RSS precisions in Table 2 for the middle and upper stratosphere but are larger at 30 and 50 hPa, presumably because of the effects of the natural variability of the atmospheric NO_2, H_2O, and temperature.

A linear scaling was applied to the entries of the V5 NO_2 error table in Russell et al. (1984a) for its V6 bias errors, based on a model-generated, daytime profile at 32° N. Its primary sources of systematic uncertainty are from temperature bias and from the interfering effects of H_2O, based on the V6 uncertainties in Remsberg et al. (2004) and Remsberg et al. (2009), respectively. There are uncertainties in the lower stratosphere due to the O_2 interference, but they should be considered as an upper limit because corrections for the O_2 emission were applied to the retrievals of both the LIMS H_2O and NO_2 and therefore carry the same sign. There is also a possible bias due to a 20% uncertainty for the area of the measured FOV side lobes; its effect on the retrieved NO_2 is believed to be small but remains unverified.

Table 2 indicates RSS V6 NO_2 uncertainties of 17% at 3 hPa and about 18% from 5 to 10 hPa. RSS values increase sharply in the lower stratosphere and are dominated by the estimates of error for the interfering O_2 continuum and the H_2O. At stratopause levels (1 hPa) the ascending (daytime) NO_2 may have a bias of order 33% across most latitudes. However, the larger, descending (nighttime) NO_2 values at that level are not affected much by the interfering H_2O, so they are more accurate (∼17%). Also, the increasing values of NO_2 in the lower mesosphere at the high northern latitudes of Fig. 3 are judged to be reasonably accurate (see also Sect. 4.4). One source of bias error that has been neglected is the likelihood that the retrieved V6 polar night NO_2 values are too low in the mesosphere due to not accounting for the effects of non-LTE emissions of the ground-state of NO_2 itself (e.g., see Funke et al., 2005a).

4 Scientific implications of the V6 data

The previously, archived LIMS V5 HNO_3 and NO_2, along with the temperature, O_3, and H_2O data have been used in scientific studies and reported in the literature (e.g., Callis et al., 1983; Jackman et al., 1985; Natarajan et al., 1986; Solomon et al., 1986; and Considine et al., 1992). In the subsections that follow several of the issues that they raised with respect to the V5 HNO_3 and NO_2 profiles and distributions are re-visited and re-evaluated using the V6 data.

4.1 HNO_3/NO_2 ratio profiles

Simultaneous measurements of HNO_3 and NO_2 by LIMS provide an opportunity to check the partitioning of NO_y species in comparison with that predicted with theoretical models. Notably, Jackman et al. (1985) reported that between 5 and 1 hPa the ratio of the LIMS V5 daytime HNO_3 to NO_2 was inconsistent with model values and that HNO_3 derived from photochemical relations should be used instead of those from LIMS. They based their conclusion on a comparison of daytime hydroxyl (OH) values derived from the V5 data using two different procedures. In the first approach they invoked an instantaneous photochemical equilibrium assumption for HNO_3 and, thereby, expressed OH concentrations as a function of the ratios of HNO_3/NO_2. Their second approach used an equilibrium assumption for odd hydrogen (HO_x) along with the LIMS O_3 and H_2O data to derive the daytime OH values. In the upper stratosphere those two approaches yielded different results. For instance, the V5 HNO_3/NO_2 ratios overestimated OH in the upper stratosphere by a large margin, at least when compared to other available observations and model results. It is noted though that the lifetime of HNO_3 against photolysis in the upper stratosphere is an hour or more, such that their instantaneous assumption is not strictly valid at the local measurement times of LIMS across all latitudes. Even so, their second approach yielded much better agreement with model OH values. Jackman et al. (1985) concluded that the problem with the first approach was due to errors in the LIMS HNO_3 in the 5 to 1 hPa region. Natarajan et al. (1986) reached a similar conclusion regarding the HNO_3/NO_2 ratio, but on the basis of diurnal photochemical model calculations that were constrained by the LIMS V5 nighttime data. The V5 HNO_3/NO_2 ratios also showed a positive bias in the upper stratosphere in comparison with their modeled daytime estimates.

Figure 6 is a comparison of the daytime ratio of V6 HNO_3/NO_2 for 15 February 1979 versus that from the updated, diurnal photochemical model of Natarajan et al. (2002), which incorporates the recommended chemical kinetics data of Sander et al. (2006). Distributions of long-lived species, such as nitrous oxide (N_2O) that are used to initialize the diurnal calculations are taken from a simulation with the NASA Langley two-dimensional model of Callis et al. (2001) using surface source gas mixing ratios corresponding to the 1978–1979 time period. The bottom panel of Fig. 6 shows LIMS HNO_3/NO_2 ratios that are less than 0.2 in the upper stratosphere to near 3 hPa, except at the winter high latitudes where the photochemical partitioning of the atmospheric NO_y to HNO_3 and NO_2 is incomplete. In addition, at the top boundary of the data domain (near 2 hPa) the V6 ratios are lower than the ones from the V5 data (not shown). The better determinations of the V6 temperature profile and its effects for the laser band of CO_2 have led to a large decrease in the retrieved, upper stratospheric HNO_3 and a corresponding decrease in the HNO_3/NO_2 ratio. The model results are shown in the top panel of Fig. 6, and they agree well with the ratios from the V6 data.

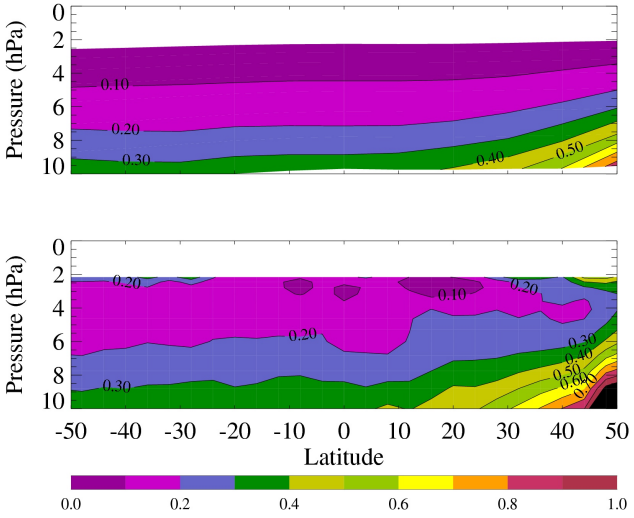

Fig. 6. HNO_3/NO_2 ratios for February 1979 – (top) model and (bottom) LIMS V6 data. Orange-to-red colors represent high ratios, while the magenta color shows low ratios.

The HNO_3/NO_2 ratios in Fig. 6 from both the model and LIMS are declining from 10 hPa to about 3 hPa, but then the LIMS ratios become larger than the model values at the topmost boundary. The reason for the remaining disagreement near 2 hPa is most likely a high bias in the daytime HNO_3 due to the influence of non-LTE emission in the spectrally-broad, LIMS channel that has not been corrected. Edwards et al. (1996) also observed differences between the day and night radiances from the 10.83-μm blocker channel of the Cryogenic Limb Array Etalon Spectrometer (CLAES) instrument, and they ascribed them to non-LTE effects from ozone and CO_2 near the stratopause during daytime. Estimates of the effects of those emissions on the retrieved LIMS HNO_3 have not been evaluated for this paper. Nevertheless, because of the improved results from LIMS V6 there is no longer any need to substitute model HNO_3 for the retrieved LIMS daytime values throughout most of the upper stratosphere.

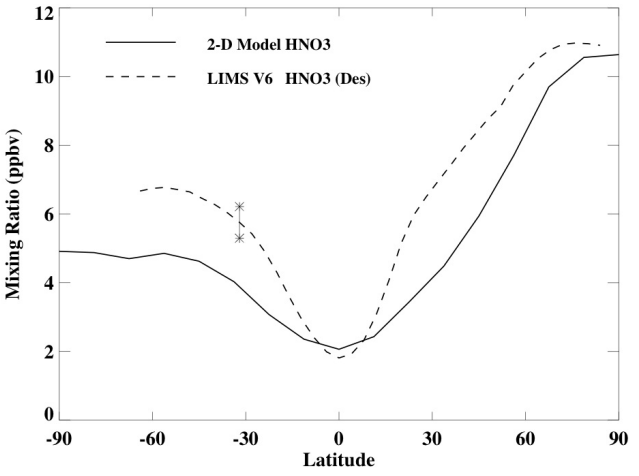

Fig. 7. LIMS V6 (dashed) and model (solid) comparisons for HNO_3 in ppbv from the LIMS descending (Des or nighttime) orbital segments of December 1978. The vertical line on the LIMS data at 32° S denotes its estimated uncertainty.

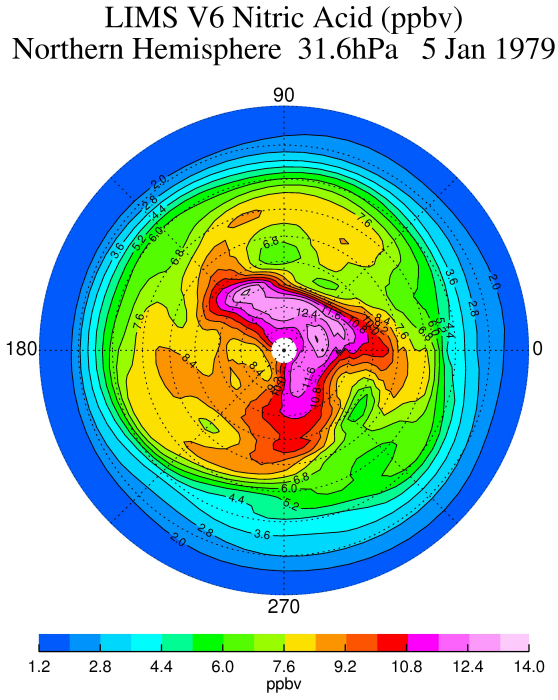

Fig. 8. Ascending plus descending V6 HNO_3 in ppbv for 5 January 1979. Bluish regions are low values and orange-to-pink regions are high values; contour interval is 0.8 ppbv.

4.2 Lower stratospheric HNO_3 and NO_2

The LIMS dataset provides global scale information on the latitudinal distribution of stratospheric HNO_3 and NO_2. Earlier analyses of the V5 data in conjunction with model studies highlighted a deficiency with respect to the HNO_3 mixing ratios of the winter high latitudes as calculated by models using only gas-phase chemistry. For instance, Austin et al. (1986) compared LIMS V5 HNO_3 with other measurements and model results. They reported that an additional source of HNO_3 was needed at high latitudes in winter and suggested that the hydrolysis of N_2O_5 on aerosol surfaces could be important. Considine et al. (1992) also described results from their two-dimensional model compared with the V5 data and noted the importance of heterogeneous chemistry for their calculations of HNO_3. They also pointed out that while the inclusion of heterogeneous chemistry improved the model/data agreement for HNO_3, its addition led to larger discrepancies between the calculated and observed NO_2.

At this point it is noted that the latitudinal variations from the V6 algorithm are similar to those from V5 for middle and lower stratospheric HNO_3 and for NO_2 (at least above the 30-hPa level). Their profile variations in the middle to lower stratosphere are also similar to the results (not shown) from more recent satellite experiments (e.g., Santee et al., 2007; Wetzel et al., 2007; Kyröla et al., 2010). These results are not surprising because the updated spectral parameters for the primary gases of V6 have little effect on their retrieved mixing ratios at those altitudes. However, changes from V5 to V6 were found in the lower stratosphere at tropical and polar winter latitudes, due to improvements in their associated profiles of $T(p)$ and interfering species.

Figure 7 shows a comparison of zonally averaged HNO_3 at 30 hPa as a function of latitude for December 1978. The dashed line represents LIMS V6 data, and the solid line corresponds to the HNO_3 from the two-dimensional model of Callis et al. (2001). The model includes heterogeneous processing of N_2O_5 and $ClONO_2$ on stratospheric sulfate aerosol surfaces, leading to the production of HNO_3. Reaction probabilities were adopted for the model from Sander et al. (2006). The surface area densities for the background aerosol distribution were taken from the climatology based on SAGE II measurements (Thomason et al., 1997). The model does not include reactions on polar stratospheric cloud particles. A heterogeneous reaction path explains the higher mixing ratios at the winter high latitudes and the good agreement with the LIMS data.

The vertical line in Fig. 7 represents the estimated LIMS uncertainty of 8% based on a mid-latitude summer profile (Table 1). It is clear that the LIMS HNO_3 is higher than that of the model across the middle latitudes and has a different slope, particularly for the winter hemisphere. Figure 8 shows the V6 HNO_3 distribution on the 31.6 hPa surface of the northern hemisphere for early January 1979, and it exhibits a zonal wave-3 variation at middle and high latitudes. Remsberg and Bhatt (1996) indicated that the effects of such zonal wave activity could lead to the pattern of the middle latitude surf zone plus a subtropical barrier region by early January, as shown in Fig. 8. It is difficult to simulate such

wave forcing and subsequent changes of the HNO_3 distribution with the parameterized transport of a two-dimensional model. Thus, while the model results indicate the proper seasonal variations at the high latitudes, they do not agree well in the middle latitudes with the early January data at this pressure level. In the tropics the observed HNO_3 in Fig. 8 displays almost no zonal variations; Fig. 7 shows that the LIMS data and model results agree well in that region.

Figure 9 is a polar plot of the northern hemisphere distribution of LIMS V6 nighttime NO_2 at 31.6 hPa for 5 January 1979. Note that the distribution shows a decrease along the 270° E meridian from about 2.4 ppbv at 30° N to less than 1.0 ppbv by about 50° N. This change is a clear indication of the so-called "cliff phenomenon" in column NO_2 over North America (Noxon, 1979). Such a pronounced variation with latitude was not as apparent and coherent within the V5 dataset. One can now readily follow the daily evolution of this feature and compare it with the changes in HNO_3 using the V6 data.

4.3 Day-to-night NO_2 ratios

The availability of daytime and nighttime measurements of a diurnally varying species like NO_2 allows one to examine the photochemistry of this species using theoretical models in conjunction with data. For example, Solomon et al. (1986) used LIMS nighttime NO_2 data at high northern latitudes in May to show that the decay of NO_2 to form N_2O_5 was consistent with theory. On the other hand, Kerridge and Remsberg (1989) examined profiles of the day-to-night ratios of NO_2 and found a region of discrepancy with theory in the upper stratosphere. In particular, the LIMS V5 data showed much larger ratios than expected from photochemical models above about 42 km (or the 2-hPa level).

An updated comparison of the day-to-night NO_2 ratio profiles from the V6 dataset is shown in Fig. 10 along with those from a contemporary, diurnal photochemical model. The model is an updated version of the zero-dimensional model described in Natarajan et al. (2002) and Natarajan and Callis (1991). The numerical procedure uses a stiff equation solver to integrate the system of species continuity equations. Chemical kinetics and photochemical data are adopted from Sander et al. (2006). For each latitude and altitude location considered, the model is constrained by the nighttime observations of LIMS. Initialization for species that are not measured by LIMS, for example chlorine species, is based on the results of the two-dimensional model of Callis et al. (2001). During initialization, the calculations are repeated for a few diurnal cycles, and in each cycle at the local time corresponding to the LIMS nighttime measurement the mixing ratios of the observed species are reset to the measured values. Once the unmeasured reactive species reach a steady diurnal variation, the time integration is continued for another diurnal cycle and the required parameters are evaluated, i.e., the day/night ratios for NO_2.

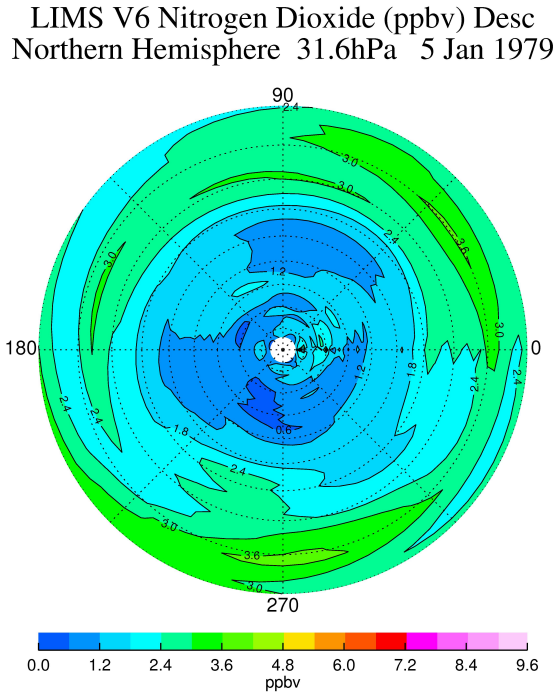

Fig. 9. V6 descending NO_2 in ppbv for 5 January 1979. Bluish regions are low values and greenish regions are high values; contour interval is 0.6 ppbv.

The monthly-averaged LIMS results for May 1979 are in the bottom panel of Fig. 10, and they show steadily declining ratios above the 5-hPa level, reaching a minimum of less than 0.05 at 1.0 hPa but then increasing to about 0.15 at 0.5 hPa. The model day-to-night NO_2 ratios are shown in the top panel and correspond to the local times of the LIMS day and night measurements. The model ratios are in good agreement with the data in the 5 to 1 hPa region but continue to show decreasing values in the lower mesosphere. Interfering radiance from H_2O is the primary source of uncertainty for the LIMS forward model of NO_2 in the mesosphere, especially for daytime. H_2O was accounted for by considering the retrieved H_2O up to 1.5 hPa plus a fixed H_2O value above that level, even though non-LTE emissions from H_2O are known to be important (Remsberg et al., 2009). As with V5, the LIMS V6 algorithm does not correct for such non-LTE effects in H_2O, leading to a positive bias in the retrieved daytime NO_2. Funke et al. (2005a) found no evidence for non-LTE emissions from the higher-vibrational states of NO_2 itself in the MIPAS data, at least for altitudes below 50 km. Whether there may be such effects from NO_2 in the lower mesosphere is unclear. It is tentatively concluded that any non-LTE effects from NO_2 in the mesosphere are secondary to the influence of the non-LTE emissions from H_2O, and it is estimated that the upper boundary region of accurate V6 daytime NO_2 values is 1.5 to 1.0 hPa.

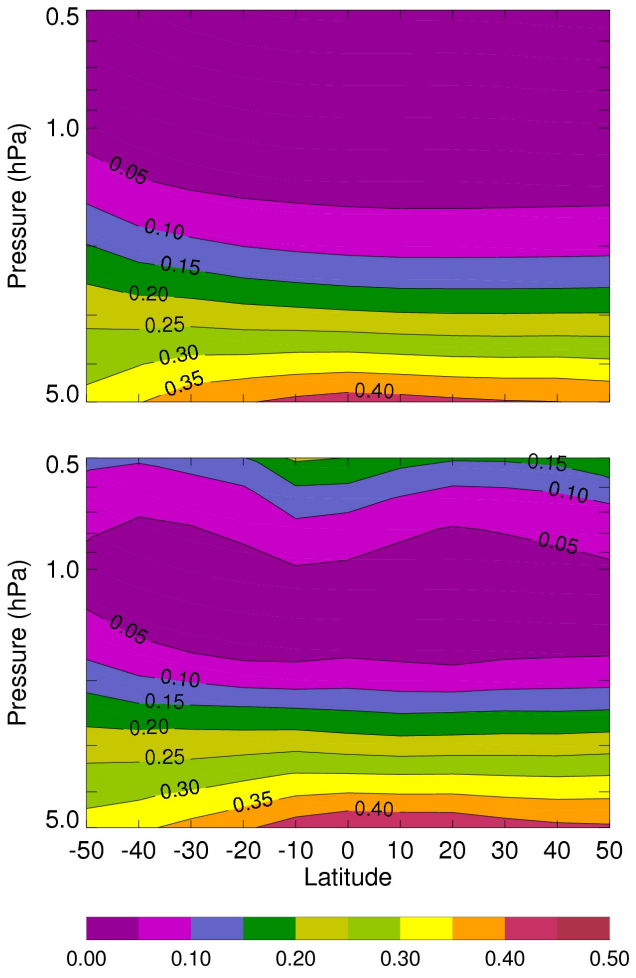

Fig. 10. Ascending/descending (or day/night) NO_2 ratio (top) from the diurnal model and (bottom) from the LIMS V6 data. Orange-to-red colors are high ratios, while magenta colors are low ratios.

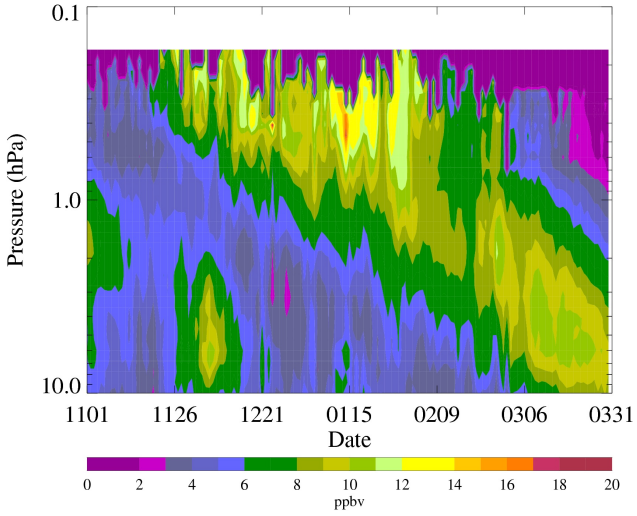

Fig. 11. Time series of LIMS V6 descending (or nighttime) NO_2 in ppbv for latitudes $>74°$ N. The time span is from 1 November 1978 (1101) to 31 March 1979 (0331). For those few days when no data were taken, the NO_2 values are averages from the adjacent days. Yellow colors are high values, while blue-to-magenta colors are low values.

4.4 Mesospheric NO_2 during polar night

The production of NO_x in the mesosphere and lower thermosphere by energetic particle precipitation has been described in connection with its downward transport into the high latitude winter stratosphere (e.g., Callis et al., 2001; Natarajan et al., 2004; Funke et al., 2005b; Randall et al., 2006). Russell et al. (1984b) reported the first satellite-based observation of wintertime increases in upper stratospheric NO_2. Upon averaging 5 days of LIMS radiances within 60° longitude sectors, they were able to extend their retrievals of LIMS NO_2 to higher altitudes. By focusing on polar night conditions in January 1979, they obtained NO_2 mixing ratios exceeding 100 ppbv in one 60° sector of the lower mesosphere. Odd nitrogen can be produced directly by solar proton events in the high latitude upper stratosphere. However, the study by Jackman et al. (1990) for the period 1963–1984 does not indicate the occurrence of any such event during January 1979. The enhanced NO_2 in the LIMS data must be due to high latitude descent within the mesosphere following the production of NO_x by energetic particle precipitation, the so-called "indirect effect" (Randall et al., 2006).

The V6 algorithm does not employ a radiance-averaging procedure, so the single profiles of V6 NO_2 extend only up to about 0.15 hPa at the winter high latitudes. Although elevated, zonally-averaged mixing ratios of NO_2 are still found in the mesosphere (Fig. 3), they are lower than those reported in Russell et al. (1984). Even so, the V6 values are considerably higher than what is expected if there are only stratospheric sources of NO_x. The occurrence of the smaller NO_2 mixing ratios from V6 is primarily because the V6 radiance profiles are registered better and the V6 temperatures are warmer by as much as 6 K at 0.1 hPa (Remsberg et al., 2004). Although the single profile error estimates for NO_2 in Table 2 apply strictly to its climatological profile and do not extend to altitudes above 1 hPa, the effects of a 2 K temperature bias and of an H_2O bias at 1 hPa are 10% and 28%, respectively. Total error in Table 2 for NO_2 is estimated to be 33% at 1 hPa. However, the EOS Aura MLS experiment confirms that H_2O has relatively small values in the wintertime, polar vortex regions of the mesosphere (http://mls.jpl.nasa.gov/). Thus, the uncertainties for the LIMS V6 NO_2 from Table 2 due to the interfering effects of H_2O should be reduced considerably for the polar night.

Figure 11 is a time series of the zonally-averaged V6 descending node (or nighttime) NO_2 mixing ratio as a function of pressure for latitudes greater than 74° N. Data from 1 November 1978 to 31 March 1979 are shown. For the

several days when the LIMS instrument did not take data, their NO_2 values are averages from the adjacent days at all pressure levels. NO_2 mixing ratios exceeding 10 ppbv occurred in the 0.2 to 0.5 hPa region from late November 1978 to early February 1979 along with a clear indication of atmospheric descent with time of that elevated NO_2. Comparisons of the fields of geopotential height and nighttime NO_2 during January at 0.46 hPa indicate that the highest NO_2 values correspond to observations within the polar vortex region (not shown). The reaction of NO_x with O_3 in the upper stratosphere leads to a gradual conversion of NO_2 to nitrogen trioxide (NO_3) and then to N_2O_5 in the polar night region. During November and December and between 2 and 10 hPa, the NO_2 variations in Fig. 11 are mostly a result of transport of air from lower latitudes followed by the photochemical conversion of its NO_2. In particular, early December 1978 was the time of a wave-1, stratospheric (Canadian) warming event. The LIMS observations of Fig. 11 provide support for the hypothesis that under such dynamic conditions there can be increases of high-latitude, upper stratospheric NO_x as a result of accelerated descent within the polar vortex. More dramatic perturbations, such as solar proton events, are not a necessary condition for moderate enhancements of upper stratospheric NO_x.

5 Summary findings

The radiances of the Nimbus 7 LIMS experiment were reconditioned and new retrievals of them conducted with an updated (V6) algorithm to generate HNO_3 and NO_2 profiles that are more compatible with those of follow-on satellite experiments. The V6 HNO_3 profiles are nearly unchanged in the middle and lower stratosphere from those of the earlier V5 algorithm. However, in the upper stratosphere V6 HNO_3 is smaller due to improvements in the accounting for interfering emissions from CO_2. That change yields daytime HNO_3/NO_2 ratios that agree better with results from theoretical model calculations than before. The V6 NO_2 profiles have smaller values than those of V5, most noticeably for nighttime in the upper stratosphere due to the accounting of spin-rotation effects within the updated, spectroscopic line parameters of NO_2. More accurate retrievals of the V6 temperature and H_2O from the lower mesosphere to near the stratopause are responsible for the more realistic V6 NO_2 profiles of that region of the atmosphere, most notably in the polar night regions. Day-to-night ratios of V6 NO_2 also agree well with photochemical model calculations in the middle and upper stratosphere.

Individual V6 profiles of HNO_3 and NO_2 have points every 0.375 km and an effective vertical resolution of 3.7 km. The V6 retrievals were applied to adjacent pairs of profiles along orbits, yielding a spacing of 1.6 degrees of latitude between retrieved profiles, on average. Single HNO_3 profiles have calculated precisions of 3–4% from 10 to 50 hPa but of order 10% at 3 hPa and 21% at 80 hPa. Single NO_2 profiles have precisions of about 3% from 3 to 10 hPa, 7% at 30 to 50 hPa, and 14% at 1 hPa. The improved precisions and more frequent retrievals of profiles along the orbit tracks provide better continuity and detail for map analyses of these two species on pressure surfaces.

Calculated accuracies for single profiles of V6 HNO_3 are better than 10% from 10 to 50 hPa, and about 12% at 3 hPa and 16% at 80 hPa. Accuracy for the V6 NO_2 profiles is of order 18% from 3 to 10 hPa, but degrades to about 30% at 30 hPa and 1 hPa. Even so, good quality retrievals of V6 NO_2 extend downward to at least the 50-hPa level at polar latitudes in northern winter, which was not the case for NO_2 from the earlier V5 dataset. A time series plot of V6 NO_2 at northern high latitudes illustrates NO_x enhancement, most likely due to wintertime descent from the lower mesosphere to the upper stratosphere. This finding is significant, especially when one considers that there were no large solar disturbances or enhanced geomagnetic storm activity in late 1978 or early 1979.

The V6 HNO_3 distributions still support the finding that one must include heterogeneous chemical mechanisms in stratospheric models for the partitioning of NO_y, even during the 1978–1979 period of low volcanic aerosol loading. However, it is also apparent from the V6 data that there are deficiencies for the seasonal, meridional transport of the N_2O source molecule and/or of its end product NO_y, as simulated with a two-dimensional model of the lower stratosphere.

The V6 Level 2 (profile) data can be obtained by ftp download from the Goddard Earth Sciences and Data Information Services Center or GES DISC (http://daac.gsfc.nasa.gov/). A LIMS V6 Level 3 or zonal Fourier coefficient product is also available at GES DISC (Remsberg and Lingenfelser, 2010).

Acknowledgements. We recognize the extensive efforts of John Gille and Jim Russell III (Co-PIs) and the members of the original Project and Science Teams for their development and conduct of the LIMS experiment. Yun-fei Wang conducted analyses of the LIMS HNO_3 radiances for evidence of any spurious effects from its FOV side lobes. The comments and suggestions from the two anonymous reviewers of the manuscript have been helpful and are appreciated. The research leading to the improvement and generation of the LIMS V6 Level 2 dataset was conducted with the consistent support of Jack Kaye of NASA Headquarters. The archival of the LIMS Level 3 product and the analyses in this manuscript were supported with funds from the NASA NRA NNH08ZDA001N of the MAP Program administered by David Considine.

Edited by: W. Lahoz

References

Austin, J., Garcia, R. R., Russell III, J. M., Solomon, S., and Tuck, A. F.: On the atmospheric photochemistry of nitric acid, J. Geophys. Res., 91, 5447–5485, 1986.

Bekki, S., Chipperfield, M. A., Pyle, J. A, Remedios, J. J., Smith, S. E., Grainger, R. G., Lambert, A., Kumer, J. B., and Mergenthaler, J. L.: Coupled aerosol-chemical modeling of UARS HNO_3 and N_2O_5 measurements in the Arctic upper stratosphere, Geophys. Res. Lett., 102, 8977–8984, 1997.

Butchart, N. and Remsberg, E. E.: The area of the stratospheric polar vortex as a diagnostic for tracer transport on an isentropic surface, J. Atmos. Sci., 43, 1319-1339, 1986.

Callis, L. B., Natarajan, M., and Lambeth, J. D.: Solar-atmospheric coupling by electrons (SOLACE) 3. Comparisons of simulations and observations, 1979–1997, issues and implications, J. Geophys. Res., 106, 7523–7539, 2001.

Callis, L. B., Russell III, J. M., Haggard, K. V., and Natarajan, M.: Examination of wintertime latitudinal gradients in stratospheric NO_2 using theory and LIMS observations, Geophys. Res., Lett., 10, 945–948, 1993.

Considine, D. B., Douglass, A. R., and Stolarski, R. S.: Heterogeneous conversion of N_2O_5 to HNO_3 on background stratospheric aerosols: comparisons of model results with data, Geophys. Res. Lett., 19, 397–400, 1992.

Dana, V., Mandin, J.-Y., Guelachvili, G., Kou, Q., Morillon-Chapey, M., Wattson, R. B., and Rothman, L. S.: Intensities and self-broadening coefficients of $^{12}C^{16}O_2$ lines in the laser band region, J. Mol. Spectroscopy, 152, 328–241, 1992.

Drayson, S. R., Bailey, P. L., Fischer, H., Gille, J. C., Girard, A., Gordley, L. L., Harries, J. E., Planet, W. G., Remsberg, E. E., and Russell III, J. M.: Spectroscopy and transmittances for the LIMS experiment, J. Geophys. Res., 89, 5141–5146, 1984.

Edwards, D. P., Kumer, J. B., Lopez-Puertas, M., Mlynczak, M. G., Gopalan, A., Gille, J. C., and Roche, A.: Non-local thermodynamic equilibrium limb radiance near 10 µm as measured by UARS CLAES, J. Geophys. Res., 101, 26577–26588, 1996.

Froidevaux, L., Allen, M., Berman, S., and Daughton, A.: The mean ozone profile and its temperature sensitivity in the upper stratosphere and lower mesosphere: an analysis of LIMS observations, J. Geophys. Res., 94(D5), 6389–6417, 1989.

Funke, B., Lopez-Puertas, M., von Clarmann, T., Stiller, G. P., Fischer, H., Glatthor, N., Grabowski, U., Hoepfner, M., Kellmann, S., Kiefer, M., Linden, A., Mengistu Tsidu, G., Milz, M., Steck, T., and Wang, D.-Y.: Retrieval of stratospheric NO_x from 5.3 and 6.2 µm nonlocal thermodynamic equilibrium emissions measured by Michelson Interferometer for Passive Atmospheric Sounding (MIPAS) on Envisat, J. Geophys. Res., 110, D09302, doi:10.1029/2004JD005225, 2005a.

Funke, B., Lopez-Puertas, M., Gil-Lopez, S., von Clarmann, T., Stiller, G. P., Fischer, H., and Kellmann, S.: Downward transport of upper atmospheric NO_x into the polar stratosphere and lower mesosphere during the Antarctic 2003 and Arctic 2002/2003 winters, J. Geophys. Res., 110, D24308, doi:10.1029/2005JD006463, 2005b.

Gille, J. C.: Distributions of ozone and nitric acid measured by the limb infrared monitor of the stratosphere (LIMS), in *Transport Processes in the Middle Atmosphere*, edited by: Visconti, G. and Garcia, R., D. Reidel Publ. Co., Dordrecht, Holland, 73–85, 1987.

Gille, J. C. and Russell III, J. M.: The limb infrared monitor of the stratosphere: experiment description, performance, and results, J. Geophys. Res., 89, 5125–5140, 1984.

Gille, J. C., Bailey, P. L., and Craig, C. A.: Revised reference model for nitric acid, Adv. Space Res., 13, 59–72, 1993.

Gille, J. C., Russell III, J. M., Bailey, P. L., Remsberg, E. E., Gordley, L. L., Evans, W. F. J., Fischer, H., Gandrud, B. W., Girard, A., Harries, J. E., and Beck, S. A.: Accuracy and precision of the nitric acid concentrations determined by the limb infrared monitor of the stratosphere experiment on NIMBUS 7, J. Geophys. Res., 89, 5179–5190, 1984.

Giver, L. P., Valero, P. J., and Goorvitch, D.: Nitric acid band intensities and band-model parameters from 620 to 1760 cm^{-1}, J. Opt. Soc. Am. B, 1, 715–722, 1984.

Goldman, A., Bonomo, F. S., Valero, F. P. J., Goorvitch, D., and Boese, R. W.: Temperature dependence of HNO_3 absorption in the 11.3-μm region, Appl. Opt., 20, 172–175, 1981.

Gordley, L. L., and Russell III, J. M.: Rapid inversion of limb radiance data using an emissivity growth approximation, Appl. Opt., 20, 807–813, 1981.

Hervig, M. E., Russell III, J. M., Gordley, L. L., Daniels, J., Drayson, S. R., and Park, J. H.: Aerosol effects and corrections in the Halogen Occultation Experiment, J. Geophys. Res., 100, 1067–1079, 1995.

Hitchman, M. A., McKay, M., and Trepte, C. R.: A climatology of stratospheric aerosol, J. Geophys. Res., 99, 20689–20700, 1994.

Jackman, C. H., Douglass, A. R., Rood, R. R., McPeters, R. D., and Meade, P. E.: Effect of solar proton events on the middle atmosphere during the past two solar cycles as computed using a two-dimensional model, J. Geophys. Res., 95, 7417–7428, 1990.

Jackman, C. H., Kaye, J. A., and Guthrie, P. D.: LIMS HNO_3 data above 5 mbar: corrections based on simultaneous observations of other species, J. Geophys. Res., 90, 7923–7930, 1985.

Jensen, E. and Drdla, K.: Nitric acid concentrations near the tropical tropopause: implications for the properties of tropical nitric acid trihydrate clouds, Geophys. Res. Lett., 29, 2001, doi:10.1029/2002GL015190, 2002.

Kawa, S. R., Kumer, J. B., Douglass, A. R., Roche, A. E., Smith, S. E., Taylor, F. W., and Allen, D. J.: Missing chemistry of reactive nitrogen in the upper stratospheric polar winter, Geophys. Res. Lett., 22, 2629–2632, 1995.

Kerridge, B. J. and Remsberg, E. E.: Evidence from the limb infrared monitor of the stratosphere for nonlocal thermodynamic equilibrium in the ν_2 mode of mesospheric water vapour and the ν_3 mode of stratospheric nitrogen dioxide, J. Geophys. Res., 94, 16323–16342, 1989.

Kyrölä, E., Tamminen, J., Sofieva, V., Bertaux, J. L., Hauchecorne, A., Dalaudier, F., Fussen, D., Vanhellemont, F., Fanton d'Andon, O., Barrot, G., Guirlet, M., Fehr, T., and Saavedra de Miguel, L.: GOMOS O_3, NO_2, and NO_3 observations in 2002–2008, Atmos. Chem. Phys. Discuss., 10, 2169–2220, doi:10.5194/acpd-10-2169-2010, 2010.

Leovy, C. B., Sun, C.-R., Hitchman, M. H., Remsberg, E. E., Russell, III, J. M., Gordley, L. L., Gille, J. C., and Lyjak, L. V.: Transport of ozone in the middle stratosphere: evidence for planetary wave breaking, J. Atmos. Sci., 42, 230–244, 1985.

Lopez-Puertas, M. and Taylor, F. W.: Non-LTE radiative transfer in the atmosphere, World Scientific Publishing Co. Pte. Ltd., London, 487 pp., 2001.

Mlynczak, M. G., Mertens, C. J., Garcia, R. R., and Portmann, R. W.: A detailed evaluation of the stratospheric heat budget 2. Global radiation balance and diabatic circulations, J. Geophys. Res., 104(D6), 6039–6066, 1999.

Natarajan, M. and Callis, L. B.: Stratospheric photochemical studies with Atmospheric Trace Molecule Spectroscopy (ATMOS) measurements, J. Geophys. Res., 96, 9361–9370, 1991.

Natarajan, M., Callis, L. B., Boughner, R. E., Russell III, J. M., and Lambeth, J. D.: Stratospheric photochemical studies using Nimbus 7 data. 1. Ozone photochemistry, J. Geophys. Res., 91, 1153–1166, 1986.

Natarajan, M., Remsberg, E. E., and Gordley, L. L.: Ozone budget in the upper stratosphere: Model studies using the reprocessed LIMS and the HALOE datasets, Geophys. Res. Lett., 29, 56–61, 2002.

Natarajan, M., Remsberg, E. E., Deaver, L. E., and Russell III, J. M.: Anomalously high levels of NO_x in the polar upper stratosphere during April, 2004; Photochemical consistency of HALOE observations, Geophys. Res. Lett., 31, L15113, doi:10.1029/2004GL020566, 2004.

Noxon, J. F.: Stratospheric NO_2. 2. Global behavior, J. Geophys. Res., 84, 5067–5076, 1979.

Perrin, A., Camy-Peyret, C., and Flaud, J.-M.: Infrared nitrogen dioxide: line parameters in the HITRAN database, J. Quant. Spectrosc. Radiat. Transfer, 48, 645–651, 1992.

Randall, C. E., Harvey, V. L., Singleton, C. S., Bernath, P. F., Boone, C. D., and Kozyra, J. U.: Enhanced NO_x in 2006 linked to strong upper stratospheric Arctic vortex, Geophys. Res. Lett., 33, L18811, doi:10.1029/2006GL027160, 2006.

Randall, C. E., Harvey, V. L., Singleton, C. S., Bailey, S. M., Bernath, P. F., Cordrescu, M., Nakajima, H., and Russell III, J. M.: Energetic particle precipitation effects on the Southern Hemisphere stratosphere in 1992–2005, J. Geophys. Res., 112, D08308, doi:10.1029/2006JD007696, 2007.

Randall, C. E., Harvey, V. L., Siskind, D. E., France, J., Bernath, P. F., Boone, C. D., and Walker, K. A.: NO_x descent in the Arctic middle atmosphere in early 2009, Geophys. Res. Lett., 36, L18811, doi:10.1029/2009GL039706, 2009.

Remsberg, E. E. and Bhatt, P. P.: Zonal variances of nitric acid vapor as an indicator of meridional mixing in the subtropical lower stratosphere, J. Geophys. Res., 101(D23), 29523–29530, 1996.

Remsberg, E. E., and Lingenfelser, G.: LIMS version 6 level 3 dataset, NASA Technical Memorandum 2010-216690, available at http://www.sti.nasa.gov, 13 pp., 2010.

Remsberg, E. E. and Russell III, J. M.: The near global distributions of middle atmospheric H_2O and NO_2 measured by the Nimbus 7 LIMS experiment, in *Transport Processes in the Middle Atmosphere*, edited by: Visconti, G. and Garcia, R., D. Reidel Publ. Co., Dordrecht, Holland, 87–102, 1987.

Remsberg, E. E., Natarajan, M., Lingenfelser, G. S., Thompson, R. E., Marshall, B. T., and Gordley, L. L.: On the quality of the Nimbus 7 LIMS Version 6 water vapor profiles and distributions, Atmos. Chem. Phys., 9, 9155–9167, doi:10.5194/acp-9-9155-2009, 2009.

Remsberg, E., Lingenfelser, G., Natarajan, M., Gordley, L., Marshall, B. T., and Thompson, E.: On the quality of the Nimbus 7 LIMS version 6 ozone for studies of the middle atmosphere, J. Quant. Spectrosc. Rad. Transf., 105, 492–518, doi:10.1016/j.jqsrt.2006.12.005, 2007.

Remsberg, E. E., Gordley, L. L., Marshall, B. T., Thompson, R. E., Burton, J., Bhatt, P., Harvey, V. L., Lingenfelser, G. S., and Natarajan, M.: The Nimbus 7 LIMS Version 6 radiance conditioning and temperature retrieval methods and results, J. Quant. Spectrosc. Rad. Transf., 86, 395–424, doi:10.1016/j.jqsrt.2003.12.007, 2004.

Remsberg, E. E., Bhatt, P. P., Eckman, R. S., Gordley, L. L., Russell III, J. M., and Siskind, D. E.: Effect of the HITRAN 92 spectral data on the retrieval of NO_2 mixing ratios from Nimbus 7 LIMS, J. Geophys. Res., 99, 22965–22973, 1994.

Rothman, L. S., Gamache, R. R., Tipping, R. H., Rinsland, C. P., Smith, M. A. H., Benner, D. C., Devi, V. M., Flaud, J.-M., Camy-Peyret, C., Perrin, A., Goldman, A., Massie, S. T., Brown, L. R., and Toth, R. A.: The HITRAN molecular database: editions of 1991 and 1992, J. Quant. Spectrosc. Radiat. Transfer, 48, 469–507, 1992a.

Rothman, L. S., Hawkins, R. S., Wattson, R. B., and Gamache, R. R.: Energy levels, intensities, and linewidths of atmospheric carbon dioxide bands, J. Quant. Spectrosc. Radiat. Transfer, 48, 537–566, 1992b.

Rothman, L. S., Goldman, A., Gillis, J. R., Tipping, R. H., Brown, L. R., Margolis, J. S., Maki, A. G., and Young, L. D. G.: AFGL trace gas compilation: 1980 edition, Appl. Opt., 20, 1323–1328, 1981.

Rothman, L. S., Rinsland, C. P., Goldman, A., Massie, S. T., Edwards, D. P., Flaud, J.-M., Perrin, A., Camy-Peyret, C., Dana, V., Mandin, J.-Y., Schroeder, J., McCann, A., Gamache, R. R., Wattson, R. B., Yoshino, K., Chance, K. V., Jucks, K. W., Brown, L. R., Nemtchinov., V., and Varanasi, P.: The HITRAN molecular spectroscopic database and HAWKS (HITRAN atmospheric workstation): 1996 edition, J. Quant. Spectrosc. Radiat. Transfer, 60, 665–710, 1998.

Russell III, J. M. and Gille, J. C.: The limb infrared monitor of the stratosphere (LIMS) experiment, in The NIMBUS 7 Users' Guide, edited by: Madrid, C. R., 71–103, NASA Goddard Space Flight Center, Greenbelt, MD., 1978.

Russell III, J. R., Gille, J. C., Remsberg, E. E., Gordley, L. L., Bailey, P. L., Drayson, S. R., Fischer, H., Girard, A., Harries, J. E., and Evans, W. F. J.: Validation of nitrogen dioxide results measured by the limb infrared monitor of the stratosphere (LIMS) experiment on NIMBUS 7, J. Geophys. Res., 89, 5099–5107, 1984a.

Russell III, J. M., Solomon, S., Gordley, L. L., Remsberg, E. E., and Callis, L. B.: The variability of stratospheric and mesospheric NO_2 in the polar winter night observed by LIMS, J. Geophys. Res., 89, 7267–7275, 1984b.

Sander, S. P., Friedl, R. R., Ravishankara, A. R., Golden, D. M., Kolb, C. E., Kurylo, M. J., Molina, M. J., Moortgat, G. K., Keller-Rudek, H., Finlayson-Pitts, B. J., Wine, P. A., Huie, R. E., and Orkin, V. L.: Chemical kinetics and photochemical data for use in atmospheric studies – Evaluation Number 15, JPL Publication 06-2, Jet Propulsion Laboratory, Pasadena, CA, 2006.

Santee, M. L., Lambert, A., Read, W. G., Livesey, N. J., Cofield, R. E., Cuddy, D. T., Daffer, W. H., Frouin, B. J., Froidevaux, L., Fuller, R. A., Jarnot, R. F., Knosp, B. W., Manney, G. L., Perun, V. S., Snyder, W. V., Stek, P. C., Thurstans, R. P., Wagner, P. A., Waters, J. W., Muscari, G., DeZafra, R. L., Dibb, J. E., Fahey, D. W., Popp, P. J., Marcy, T. P., Jucks, K. W., Toon, G. C., Stachnik, R. A., Bernath, P. F., Boone, C. D., Walker, K. A., Urban,

J., and Murtagh, D.: Validation of the Aura Microwave Limb Sounder HNO_3 measurements, J. Geophys. Res., 112, D24S40, doi:10.1029/2007JD008721, 2007.

Solomon, S., Russell III, J. M., and Gordley, L. L.: Observations of the diurnal variation of nitrogen dioxide in the stratosphere, J. Geophys. Res., 91, 5455–5464, 1986.

Stiller, G. P., Mengistu Tsidu, G., von Clarmann, T., Glatthor, N., Höpfner, M., Kellmann, S., Linden, A., Ruhnke, R., Fischer, H., Lopez-Puertas, M., Funke, B., and Gil-Lopez, S.: An enhanced HNO_3 second maximum in the Antarctic midwinter upper stratosphere 2003, J. Geophys. Res., 110, D20303, doi:10.1029/2005JD006011, 2005.

Thibault, F., Menoux, V., LeDoucen, R., Rosenmann, L., Hartmann, J.-M., and Boulet, C.: Infrared collision-induced absorption by O_2 near 6.4 µm for atmospheric applications: measurements and empirical modeling, Appl. Opt., 36, 563–567, 1997.

Thomason, L. W., Poole, L. R., and Deshler, T.: A global climatology of stratospheric aerosol surface area density deduced from Stratospheric Aerosol and Gas Experiment II measurements: 1984–1994, J. Geophys. Res., 102, 8967–8976, 1997.

Toth, R. A.: High-resolution measurements and analysis of $^{14}N^{16}O_2$ in the [001]–[000] and [011]–[010] bands, J. Opt. Soc. Am. B, 9, 433–461, 1992.

Wetzel, G., Bracher, A., Funke, B., Goutail, F., Hendrick, F., Lambert, J.-C., Mikuteit, S., Piccolo, C., Pirre, M., Bazureau, A., Belotti, C., Blumenstock, T., De Mazière, M., Fischer, H., Huret, N., Ionov, D., López-Puertas, M., Maucher, G., Oelhaf, H., Pommereau, J.-P., Ruhnke, R., Sinnhuber, M., Stiller, G., Van Roozendael, M., and Zhang, G.: Validation of MIPAS-ENVISAT NO2 operational data, Atmos. Chem. Phys., 7, 3261–3284, doi:10.5194/acp-7-3261-2007, 2007.